



Phyto-fabrication of AgNPs using leaf extract of *Vitex trifolia*: potential to antibacterial, antioxidant, dye degradation, and their evaluation of non-toxicity to *Chlorella vulgaris*

Ragavendran Chinnasamy^{1,2} · Kamaraj Chinnaperumal³ · Priyadharsan Arumugam² · Murugan Natarajan¹ · Balasubramani Govindasamy⁴ · Krithikadatta Jogikalmat² · Tijo Cherian⁵ · Jothimani Kannupaiyan⁶ · Santhosh Sigamani⁷ · Peijnenburg Willie^{8,9}

Received: 12 September 2022 / Revised: 22 December 2022 / Accepted: 22 December 2022 / Published online: 4 January 2023
© The Author(s), under exclusive licence to Springer-Verlag GmbH Germany, part of Springer Nature 2023

Abstract

The study assessed the bactericidal effects of green rapid biogenic synthesis of *Vitex trifolia* leaves AgNPs on MDR bacteria. The synthesis of AgNPs is indicated by a color change from yellow to dark brown. The ultra-visible spectrophotometer displays AgNPs at 430 nm max. This demonstrates that ions (Ag^+) were converted to silver (Ag), indicating the formation of silver nanoparticles. The synthesized nanoparticles were confirmed by their crystalline nature, shape, size, and functional groups via Fourier transform infrared spectroscopy (FTIR), X-ray diffraction (XRD), energy dispersive X-ray spectroscopy (EDAX), and transmission electron microscopy (TEM). Biomolecules contain aqueous *Vitex* extract for capping and reducing the AgNPs. The nanoparticles have a face-centered cubic structure (FCC) crystallized. The antibacterial activity against *Staphylococcus aureus*, *Vibrio cholerae*, and *Klebsiella pneumoniae* exhibited a maximum zone of growth inhibition at 75 $\mu\text{g/mL}$. The minimum inhibitory concentration (MIC) and minimum bactericidal concentration (MBC) of AgNPs against the clinically isolated pathogen *S. aureus* were 3.12 $\mu\text{g/mL}$ and 4.5 $\mu\text{g/mL}$. Furthermore, time-dependent killing kinetic experiments showed that a 6 h AgNPs treatment was sufficient to fully inhibit all bacterial growth. AgNPs at a concentration of 250 $\mu\text{g/mL}$ demonstrated antioxidant activity as measured by the FRAP and DPPH tests (85% and 90%, respectively). AgNPs demonstrated efficient photocatalytic activity in the degradation of methylene blue (MB) and achieved their highest photocatalytic activity (95%) after 2.30 h. Besides, the synthesis of AgNPs was targeted towards *C. vulgaris* algae, and exhibited deleterious effects even at larger concentrations. The chosen AgNPs concentration reduced chlorophyll, impeded algal development, and damaged the whole membrane system, as evidenced by the increased electrolyte leakage and malondialdehyde (MDA) and glutathione s-transferase (GSH) content after AgNPs exposure. Our report demonstrates that AgNPs *V. trifolia* have promising antibacterial, antioxidant, and potential dye degradation activities and can be employed in biomedical applications.

Keywords *Vitex trifolia* · Antibacterial activity, Antioxidant · Dye degradation potential · TEM · Ecotoxicity

Highlights

- The synthesized silver nanoparticles had strong antibacterial activity against clinical pathogens.
- Promising antioxidant assay exhibited DPPH and FRAP.
- Photocatalytic activity of MB was evaluations in presence of AgNPs with sun light irradiation method.
- Low toxic effects on *Chlorella vulgaris*.

✉ Ragavendran Chinnasamy
ragavan889@gmail.com

Extended author information available on the last page of the article

1 Introduction

Nanoparticles (NPs) have recently gained momentum as a result of their numerous beneficial applications in a variety of fields over the last few years, including biology, medicine, physics, chemistry, and material science [1]. Silver nanoparticles (AgNPs) have attracted curiosity among noble nanoparticles in food, cosmetics, and beverage applications [2, 3]. On the other hand, AgNPs have demonstrated excellent antimicrobial, anticancer, antiviral, antiplatelet, and anti-inflammatory effects despite having minimal toxicity, bioavailability, and biodegradability [4]. NPs can be produced in

a variety of methods, such as chemical methods, photochemical reduction, and laser excision [5, 6]. However, there are a variety of different methods for synthesizing these particles, some of which use non-biodegradable chemicals and are therefore more expensive. Alternative methods need to search for which approach is cheaper and more eco-friendly [7]. The most recent literature demonstrated a passion for employing *Belladonna* [8], *Oscillatoria sancta*, and other green path plants to synthesize AgNPs [9].

Synthesis of nanoparticles using phyto-extracts is a clean, environmentally friendly, less hazardous, and cost-effective way of manufacturing nanoparticles of diverse shapes, sizes, and morphology [10]. Many plants have important biomedical applications because their stems contain biologically active phytochemicals such as polyphenols, flavonoids, terpenoids, alkaloids, and saponins. As a result, a long list of plant species extracts has been developed in recent decades, including *Camellia sinensis* [11], *Murraya koenigii*, *Azadiracta indica* [12], *Moringa oleifera* [13], *Psidium guajava* [14] were utilized to convert of ions to iron metal nanoparticles, and they were used in environmental contaminant remediation and biomedical applications. *Vitex trifolia* L. (Labiatae) is a tropical shrub widespread in Pacific-Asian countries such as India, China, Sri Lanka, the Philippines, Indonesia, and North Australia [15]. The stem of *V. trifolia* is used for the treatment of dysentery [16], larvicidal [17], antibacterial [18], HIV type 1 reverse transcriptase inhibitory activity [19], cytotoxicity [20], and antipyretic [21].

Water contamination by various organic outflows from the textile industry, paints, cosmetics, and food processing sectors has recently received a lot of attention due to the health risks they bring to humans and other living species [22, 23]. The release of effluents containing low-biodegradable dyes into bodies of water is problematic due to their color and the hazardous by-products produced through hydrolysis and oxidation processes in the wastewater phase [24, 25]. Photocatalytic degradation of organic contaminants has received a lot of interest among the various methods for treating dye-contaminated water [26]. Traditional technologies for wastewater treatment, such as adsorption, coagulation, electrochemical oxidation, flocculation, and precipitation not only demand lengthy operation times but also produce secondary sludge that is costly to dispose of properly [27].

Nanomaterials such as metals and metal oxides in nano-dimensions have drawn a lot of attention in recent years due to their potential usage in a wide range of applications, such as photocatalytic dye degradation [28, 29]. Many transition metal nanoparticles, such as silver, titanium, gold, copper, palladium, and zinc, have been investigated for their performance in dye degradation [30–32]. The interaction with molecular oxygen in water and the production of free

radicals are driven by the collective oscillations of electrons carried on by the surface plasmon resonance (SPR) effect as they shift from the outermost band to a higher energy state. The adsorbed dye is diminished when positive holes formed by electron excitation take an electron from them [33]. Additionally, other free radicals produced from the oxidation of H^+ ions generated by the dissociation of water molecules then proceed to oxidize the dye [34]. Silver nanoparticles (AgNPs) are attracting attention for photocatalytic applications due to their low toxicity, abundance on Earth, and perfect physicochemical and spectroscopic features [2]. Ag nanoparticles have been used in various technological applications, such as catalysis, ceramics, coatings, electronics, and pharmaceuticals [35, 36].

Ag toxicity in aquatic ecosystems is widely known [37], and AgNPs have been studied to induce toxicity to a range of various organisms: bacteria [38], algae and invertebrates [39], and fish [40]. Microalgae species play a significant role in the primary production of marine ecosystems and have the ability to transport metals and other pollutants through the marine food chain [41]. Additionally, the majority of ecotoxicological evaluations of manufactured nanoparticles are limited to freshwater species employed in regulatory testing (i.e., OECD, ISO). *Chlorella vulgaris* is a non-motile reproductive cell (autospore) that reproduces asexually and rapidly. Unicellular green algae are widely distributed in freshwater, lakes, and rivers [42]. The freshwater algae due to their high sensitivity to bio-fabricated nanomaterials and maximum bioaccumulation capability can be utilized as a pollution indicator in marine bionetwork [43]. The aim of the present study is focused on *Vitex trifolia* mediated synthesis of silver nanoparticles (AgNPs), spectral characterization, and biomedical applications. (i) Antibacterial activity tested against multidrug-resistant bacteria (MDR bacteria), (ii) performed the antioxidant DPPH and reducing power assay, (iii) synthesized AgNPs were evaluated for the degradation of methylene blue under solar irradiation, (iv) examine the toxicity of AgNPs to freshwater algae *C. vulgaris* (chlorophyll content, antioxidant malondialdehyde (MDA) and glutathione s-transferase (GSH) assay).

2 Materials and methods

2.1 Collection of *Vitex trifolia*

Healthy leaves of *Vitex trifolia* (latitude 11.2485° N, longitude 78.3387° E) were collected from Kolli Hills, Salem, Tamil Nadu, India (Fig. 1). The sample was deposited in the Natural Drug Research Laboratory, School of Biosciences, Periyar University for future reference.



Fig. 1 Close view of *Vitex trifolia*

2.2 Preparation of aqueous extract

V. trifolia leaves were collected and cleaned twice under running tap water before being chopped into small pieces. It was dark-dried for 15 days at room temperature. Plant materials were completely dried and sieved with a 40- μ m mesh using a mechanical blender. Ten grams of leaf powder was added to 100 mL distilled H₂O and boiled for 25 min at 80 °C. Aqueous extract was obtained using Whatman No.1 filter paper. The pure aqueous filtrate was collected in a 200 mL conical flask and kept at 4 °C until further study [44].

2.3 Synthesis of AgNPs was confirmed by UV–Vis spectroscopy

The plant's aqueous extract was diluted with 90 mL of 1 mM AgNO₃ solution, and the mixture was then incubated for 24 h in the dark. The solution's color turned from green to brown, showing the synthesis of AgNPs. The UV-spectra of the reaction solution confirmed the reduction of Ag⁺. The AgNPs were then recovered from the mixture by high-speed centrifugation for 15 min at 10,000 rpm. The produced AgNPs pellets were centrifuged, then rinsed with 15 mL of dH₂O, free-dried, and stored at room temperature for further research [45]. The synthesis of AgNPs in a solution was measured by UV–Vis spectroscopy. The UV–visible spectrum was obtained from 200 to 700 nm. Blank was a silver nitrate solution.

2.4 Structural and functional AgNPs

After purification, biosynthesized AgNPs were studied via FTIR, XRD, EDX, TEM (SAIF) at IIT, Madras. The functional bioactive compounds in the *V. trifolia* aqueous extract that served as reducing and stabilizing agents for the green production of AgNPs were identified using FTIR analysis. The FTIR spectrum was acquired with a Bruker RFS MultiRAM, 3000 Hyperion microscope with FTIR equipment. XRD with CuK α radiation was used to determine the crystalline structure of the produced AgNPs. High-resolution electron microscopy (HR-TEM) images captured the particle's deep morphology, shape, and particle size (JOEL, Japan). UV–vis spectrophotometer examined AgNPs optical absorption (Perkin Elmer Lambda 19) [46].

2.5 Isolation and identification of MDR bacteria

The isolation of multidrug-resistant bacteria (MDR) (from clinical sources) was investigated by standard protocols of the Clinical and Laboratory Standards Institute (CLSI-2012). The preliminary isolation and identification of multidrug-resistant bacteria, viz., *Streptococcus pyogenes*, *Vibrio cholerae*, *Escherichia coli*, *Staphylococcus aureus*, and *Klebsiella pneumoniae* isolated from different samples based on standard tests. The cultures were obtained from the Department of Microbiology, Mohan Kumaramangalam Medical College, Salem, Tamil Nadu, India. All the isolated microbes were maintained by glycerol stocks for further analysis [47].

2.5.1 Antibiotics susceptibility test

The susceptibility of all isolated MDRB's is tested for antibacterial potential using standard and commercially available antibiotics by the modified Kirby-Bauer disc diffusion method [48].

2.5.2 Screening of antibacterial activity

Preparation of the media containing 150 mL of distilled water, 5.7 g of Muller-Hinton agar, and 0.75 g of agar were added. The medium was added to the petri plate after it had been autoclaved, and it was then allowed time to cool. The cotton swab was immersed in the culture suspension. Five wells are created on a petri plate using a cork borer. Three of these wells contain various concentrations of silver nanoparticle treatment, whereas the other two contain antibiotic positive and aqueous extract negative controls, respectively. To evaluate the antibacterial property of

nanoparticles, the plates are incubated overnight at 37 °C, with the inhibition zone being recorded in mm [49].

2.5.3 Minimum inhibitory concentration

The MIC of AgNPs was determined using broth microdilution. Two-fold serial dilutions of silver nanoparticles (19–100 µg/mL) and antibiotics were prepared in Mueller–Hinton broth. Each well was inoculated with 5 µL (5×10^8 CFU/mL) and incubated at 37 °C for 20 h. The MIC value represents the lowest concentration, having effectively inhibited the growth of bacteria. To confirm MIC, a loopful of inoculum from each well with no noticeable growth was spotted on MHA plates. Each experiment was carried out in triplicate [50].

2.5.4 Minimal bacterial concentration

The conventional approach was used to calculate particle bactericidal concentrations (MBC). MBC values were obtained by sub-culturing MIC dilutions on sterile Muller–Hinton agar plates at 37 °C for 24 h. MBC is the lowest dose of nanoparticles required to kill the tested bacteria. The MBC value correlated with the concentration at which 100% of bacterial growth was prevented when compared to the positive control (no treatment). All experiments were done in biosafety cabinets [51].

2.6 Cellular content measurement

2.6.1 Protein leakage assay

The bacterial cells were exposed to various concentrations of silver nanoparticles for about 3, 6, 9, and 12 h. After that, 200 µL of each sample's supernatant was combined with 800 µL of Bradford reagent, and the mixture was allowed to incubate for 10 min. The optical measurements were carried out at 595 nm. The experiment was conducted in triplicate, and bovine serum albumin was employed as the reference protein [52].

2.6.2 Nucleic acid leakage assay

At 3- and 6-h intervals, aliquots (3 mL) of bacterial cultures were exposed to AgNPs. It was then filtered with a 25 mm × 0.2 m Millex-GS-Syringe filter. The quantity of nucleic acids in the solution was evaluated by measuring absorbance at 260 nm [53].

2.6.3 *In vitro* killing assay

Bacteria were grown overnight in MHB broth, then regrown in fresh medium for 4 h before being suspended in dH₂O.

This method was chosen because deionized water does not include the chloride ions found in PBS, which would interact with the silver [54]. The cells were treated with AgNPs and antibiotics (Positive control) for 4 h at 37 °C. Following the proper time points for collecting the bacteria, 100 µL of aliquots from each sample were collected to measure the CFUs, indicating a positive control (AgNPs and MHB media without inoculum) and a negative control (MHB and inoculum without AgNPs) served as the samples. All samples were replicated [55].

2.7 Antioxidant assay

2.7.1 DPPH radical scavenging assay

The spectrophotometric approach can be used to assess the free radical scavenging activities of test samples of *V. trifolia* aqueous extract and synthesized AgNPs by assessing the change in absorbance of DPPH (1, 1-diphenyl-2-picrylhydrazyl radical) at 517 nm [56]. DPPH is a stable free radical that can accept an electron or hydrogen radical to produce a diamagnetic molecule. The sample's radical scavenging potential was evaluated by DPPH at 517 nm. After 30 min, the final solution's absorbance was 517 nm.

2.7.2 Ferric reducing antioxidant power (FRAP)

The antioxidant power of *V. trifolia* aqueous extract and fabricated AgNPs was measured by following the modified protocol of Manimaran et al. [56]. This method measures the absorbance of the ferric-tripyridyltriazine (TPTz) complex to its ferrous-colored form in the presence of antioxidants. In a summary, different doses of *V. trifolia* aqueous extract and synthetic AgNPs (50–250 µg/mL) were combined with acetate buffer (2.5 mL, 0.3 M, pH 3.6) and potassium ferricyanide (2.5 mL, 1%). The mixture was incubated at 37 °C for 30 min. 2.5 mL of 10% trichloroacetic acid was added to the mixture, and its supernatant was mixed with distilled water (2.5 mL) and 0.1% FeCl₃ (0.5 mL). The absorbance was measured at 593 nm. Increased reducing power is shown by increased reaction mixture absorbance. The baseline used was ascorbic acid.

$$\% \text{ Scavenging activity} = \frac{\text{Absorbance control} - \text{Absorbance sample}}{\text{Absorbance control}} \times 100$$

2.8 Photocatalytic dye degradation

Under sunlight irradiation, green synthesized AgNPs have been evaluated for the photocatalytic degradation of methylene blue, which acts as an excellent source for photocatalytic potential. The dye solutions (stock) were prepared by adding

dyes at a concentration of 5 mg/L in a bottle, and the prepared solutions were stirred for 45 min at room temperature. To prepare stock, 5 mg of AgNPs were added to 50 mL of dye solution. The dye and nanoparticle mixture were maintained under the stirring conditions for 45 min and exposed to sunlight. The mixture was then subjected to exposure to sunlight for 6 h, and 3 mL of mixture was collected at different time intervals (every 20 min) and centrifuged at 10,000 rpm for 10 min. The collected supernatant was measured using UV–visible spectroscopy to calculate the degradation of dye. The dye degradation rate was assessed using the following formula:

$$\text{Decolorization efficiency(\%)} = \frac{C_o - C}{C} \times 100$$

C_o : initial concentration of the dye solution.

C : concentration of the dye solution after “t” minutes of exposure to sunlight.

2.9 *Chlorella vulgaris* exposed to synthesized *V. trifolia* AgNPs

2.9.1 Culture collection and maintenance

Pure cultures of *Chlorella vulgaris* were collected from the Department of Microbiology, School of Biosciences, Periyar University, Salem, Tamil Nadu, India. The algal cells were cultivated in BG-11 medium at 26 ± 0.5 °C with fluorescent lamps (about 2500 lx) for a 12-h light and 12-h dark photoperiod each day. The culture flasks were rotated 3 to 4 times per day to achieve a homogeneous combination of the contents. Algal cell proliferation was evaluated using a hemocytometer and the absorbance at OD₆₈₀. The *Chlorella* species selected for this research were identified using morphological features [57].

2.9.2 Test for algal growth inhibition

The effect of *V. trifolia* AgNPs synthesized on the growth of *C. vulgaris* was tested using the OECD 201 methodology for freshwater algae [58, 59]. In a 500-mL conical flask, the starting cell density was increased to 2×10^6 cells mL⁻¹, and the AgNPs were incubated for 96 h with aeration to minimize clumping. The optical density at 650 nm was recorded at the end of the experiment to determine the algal density. The average growth rate was Eq. (1), and the growth inhibition (%) for each AgNPs concentration was determined as Eq. (2).

$$\mu (i - j) = \ln X_j - \ln X_i / t_j - t_i \text{ (day} - 1) \quad (1)$$

where, $\mu (i - j)$ is the average specific growth rate from time i to j ; X_i and X_j are the biomass at time i and j , respectively.

$$\%Ir = \mu_c - \mu_t / \mu_c \times 100 \quad (2)$$

where, μ_c and μ_t are precise growth rates in control and treatment groups, respectively, for each of the *V. trifolia* synthesized AgNPs tested in the research.

2.9.3 Estimation of pigment contents

To assess chlorophyll (Chl *a*, *b*) content, each treated group's 40 mL *C. vulgaris* culture was centrifuged at 9000 g for 12 min. Algal debris was collected, suspended in DMF (N, N-dimethylformamide) and left at 4 °C in the dark for a day. The chlorophyll content of the extract supernatant was measured at 649 nm and 665 nm [60, 61].

$$\text{Chl } a = 13.7 \times \text{OD}_{665} - 5.76 \times \text{OD}_{649}$$

$$\text{Chl } b = 25.8 \times \text{OD}_{649} - 7.6 \times \text{OD}_{665}$$

2.9.4 Antioxidant enzyme assay

For the antioxidant enzyme assay, 200 mL of algal cultures were centrifuged at 10,000 g for 20 min at 4 °C after 96 h of exposure to different doses of AgNPs. Prior to enzyme extraction, the pellet containing the algal cells was twice washed [62]. The supernatant was used for lipid peroxidation and anti-oxidative enzymatic assays (MDA) [63] and a reduced glutathione s-transferase (GSH) assay [64]. Enzyme activity was used to measure antioxidant activity.

2.10 Statistical analysis

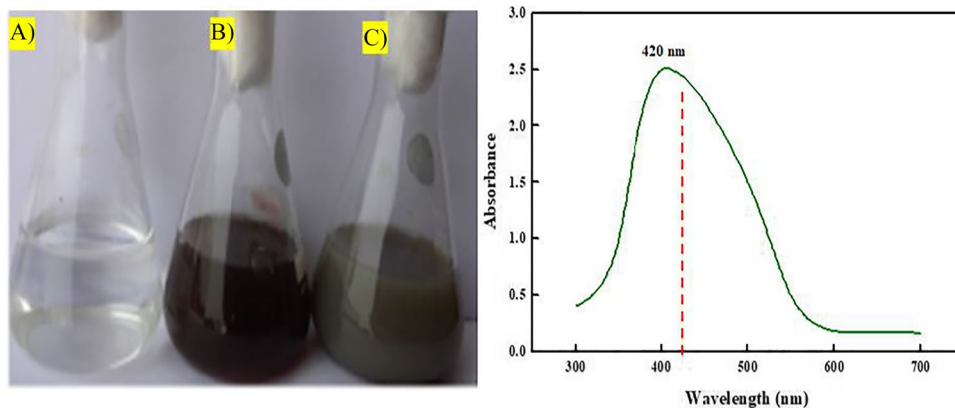
The statistical analysis was performed using a two-way ANOVA. Single asterisk (*) indicates $p < 0.01$ difference between positive control (ascorbic acid) and test samples, double asterisk (**) at $p < 0.001$. All experiments were done twice, with two replicates per treatment. Data was mean standard error (SE).

3 Results

3.1 Fabrication of silver nanoparticles

The aqueous leaf extract of *V. trifolia* was used to succeed in the fabrication of AgNPs at a concentration of 1 mM AgNO₃. Before adding AgNO₃, the aqueous extract was yellow. However, adding 1 mM AgNO₃ initially caused no color change. After 3 h in a dark environment, the solution turned dark brown, indicating AgNPs formation. The surface plasma resonance observed at a single peak at 430 nm and

Fig. 2 UV–Vis spectral analysis of synthesis of AgNPs, **A)** 1 mM AgNO₃, **B)** *V. trifolia* aqueous extract, **C)** fabrication of AgNPs



the absorption spectrum of *V. trifolia* leaf extract confirm the production of AgNPs (Fig. 2A–C).

3.2 Fourier transform infrared (FTIR)

The vibration of the spectral peaks can be used to estimate the number of functional groups that are present in the aqueous extract and nanoparticles. The absorbance bands observed in the region of 400–4000 cm⁻¹ are 3361.75, 2916.35, 2848.98, 2363.49, 1613.78, 1382.98, and 1052.41 cm⁻¹ and the synthesized AgNPs 3419.51, 2932.73, 2426.27, 1623.90, 1383.45, 1089.16, 826.44, 653.23 cm⁻¹. The absence of a spectrum (3419.51 cm⁻¹) in the *V. trifolia* extract compared to synthesized AgNPs and the alteration exhibited in the peaks supported the interaction of functional groups in the reduction process. The bands in the FTIR spectra from 3419.51 cm⁻¹, which correspond to O–H stretching vibration, confirm the presence of alcohol and phenol. According to a report, silver ions and hydroxyl groups (O–H) have a greater propensity to bind [65]. The band at 3361.75 is due to stretching O–H groups in water, alcohol, or phenols. A peak at 2916.35 cm⁻¹ owing to C–H stretching in alkanes and at 2848.98 cm⁻¹ due to carboxylic acids. The coordination of bonds, 1613 cm⁻¹ N–H bend,

primary amines, 1382 cm⁻¹ C–X fluoride, and 1052 cm⁻¹ C–N stretch can be used to explain the mechanism of adsorption and capping of silver nanoparticles by *V. trifolia*. Aliphatic amines are also responsible for the reduction of silver nitrate ions. Our results' FTIR signatures suggest that the soluble components in the aqueous extract that include a large proportion of C–N, C–H, and O–H groups serve as capping and stabilizing agents for nanoparticles (Fig. 3A) and B); Table 1).

3.3 XRD, EDX, and TEM analysis of fabricated AgNPs

The face-centered cubic crystal (fcc) structure had the Bragg's reflection visible at its 37.84°, 44.08°, 64.36°, and 77.34° facets. The average grain size of fabricated AgNPs was 20 nm when 1.5404 Å was substituted into Scherrer's formula $D = (0.9 \times 180) / \beta \cos \theta$. The XRD analysis's conclusion that bioactive compounds in *V. trifolia* extract converted silver-to-silver metal is supported by this data (Fig. 4a)). Energy dispersive X-ray fluorescence analysis was used to demonstrate that silver was a significant component of the particles and that there were strong signs of elemental silver present (Fig. 4b)). Silver ions in *V. trifolia* had 30 keV peaks. Furthermore, AgNPs were found in leaf extraction as well as a few additional peaks, as shown

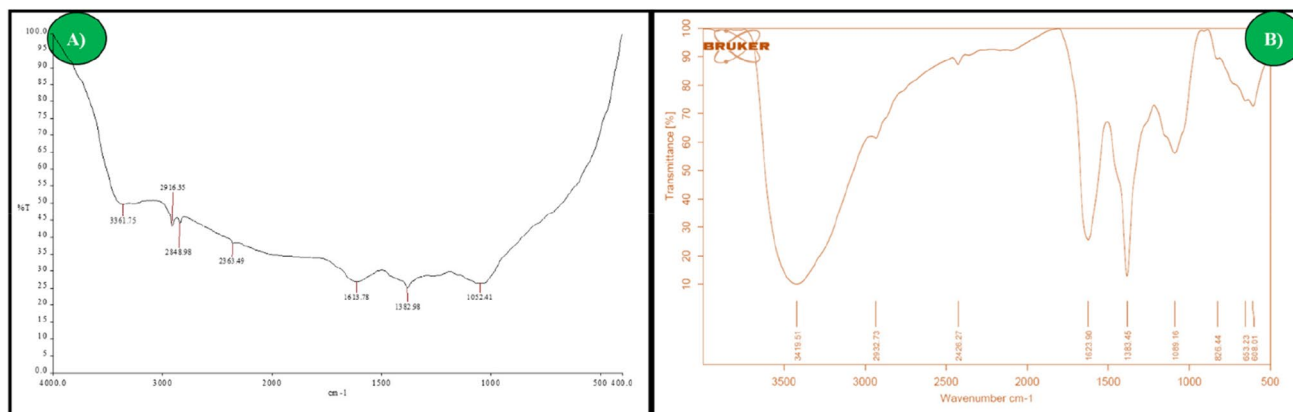


Fig. 3 **A)** FTIR spectrum of *V. trifolia* aqueous extract and **B)** FTIR spectrum of synthesized AgNPs

Table 1 FTIR analysis of functional groups are detected in aqueous extract and synthesized AgNPs

Aqueous extract of <i>V. trifolia</i>			
S. no	Observed wave number (cm ⁻¹)	Vibration assignment/functional groups	Visible intensity
1	3361.75	N–H stretch, 1°, 2° amines amides	Medium
2	2916.35	C–H stretch, alkanes	Medium
3	2848.98	O–H stretch, carboxylic acid	Medium
4	1613.78	N–H bend, 1° amines	Medium
5	1382.98	C–X, fluoride	Strong
6	1052.41	C–N stretch, aliphatic amines	Medium
Synthesized AgNPs			
1	3419.51	O–H stretch, alcohol or phenols	Medium
2	2932.73	=C–H stretch, alkenes	Medium
3	2426.27	O–H stretch, carboxylic acid	Medium
4	1623.90	N–H bend, 1° amines	Medium
5	1089.16	C–N stretch, aliphatic amines	Medium
6	826.44	=C–H bend, alkenes	Medium

by the EDX spectra for the Ag. Results show that fabricated nanoparticles are high-purity AgNPs. The TEM profile of fabricated AgNPs by fresh *V. trifolia* leaf extract exhibited poly-dispersed, spherical in shape with smooth surface morphology.

The average nanoparticle size was 50 nm. Only a few of the silver nanoparticles showed clusters of different sizes; the majority were widely scattered (Fig. 4c)).

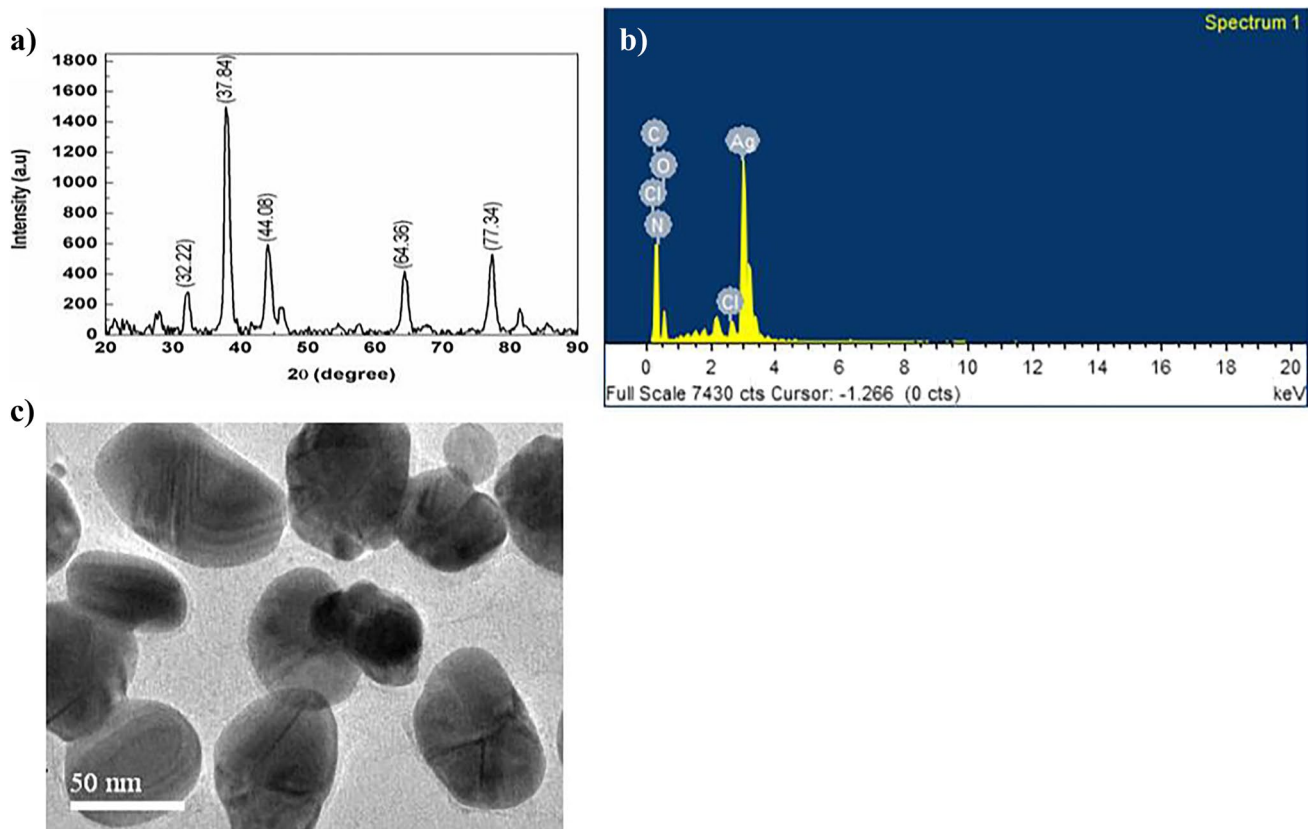


Fig. 4 Characterization of synthesized AgNPs **a)** XRD analysis of AgNPs, **b)** energy dispersive X-ray analysis (EDX), **c)** TEM analysis of fabricated AgNPs

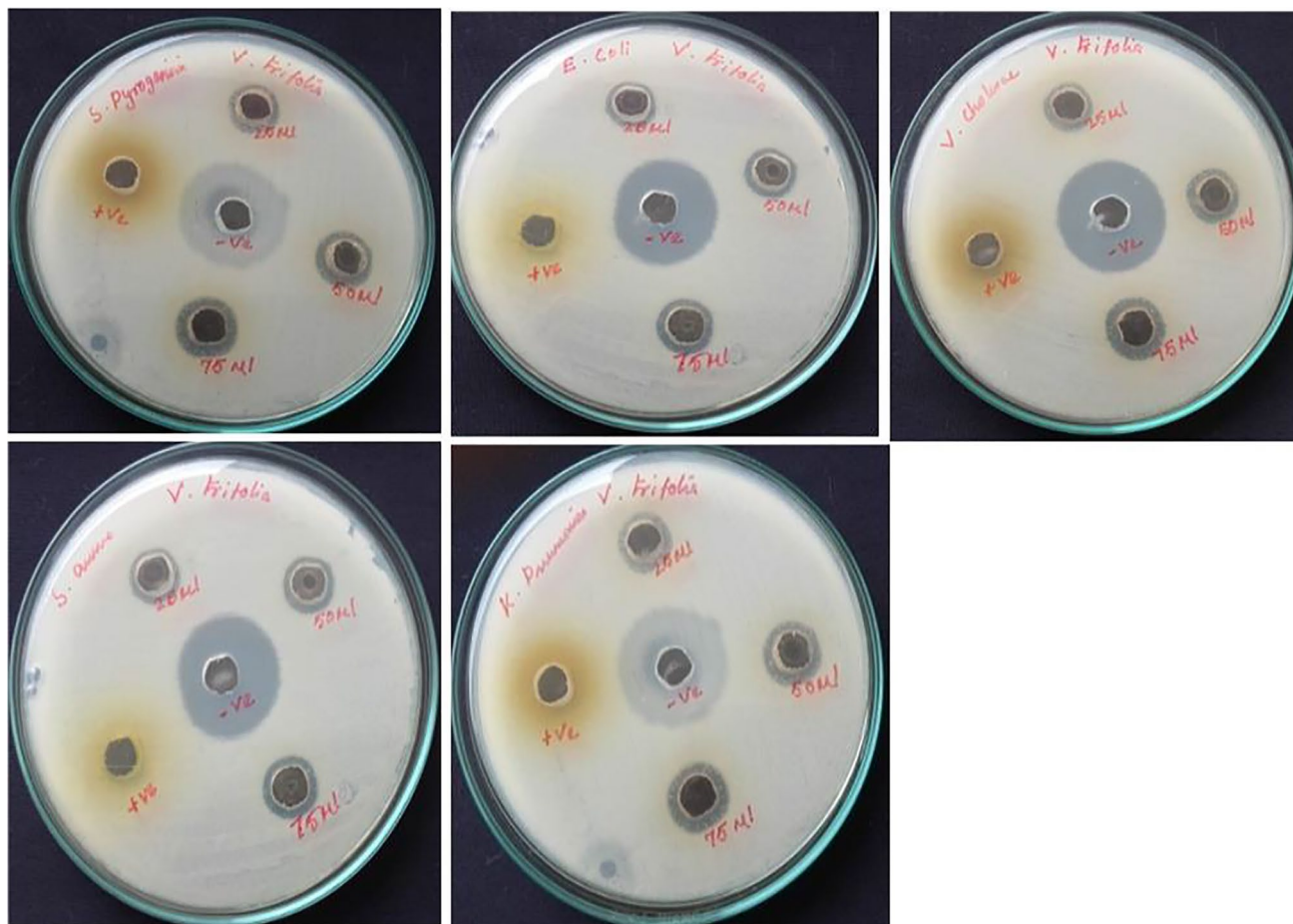


Fig. 5 Antibacterial activity of *V. trifolia* leaf extract mediated AgNPs against-multi drug resistant bacteria's (*S. pyogenes*, *E. coli*, *V. cholerae*, *S. aureus*, and *K. pneumoniae*)

3.4 Antibacterial activity

The antibacterial activity of silver nanoparticles was demonstrated by the formation of inhibitory zones of various widths in Fig. 5. The findings of the antibacterial test (the diameters of the zone of inhibition) were presented in (Table 2). The silver nanoparticles were found to be the most efficient

against *V. cholerae* (18 ± 0.8 mm), *S. aureus* (16 ± 0.4 mm), *K. pneumoniae* (17 ± 0.4 mm), *E. coli* (15 ± 0.9 mm), and *S. pyogenes* (16 ± 0.0 mm). The negative control sample contains exclusively plant extract zone of inhibition 07 mm and positive control (chloramphenicol) exhibited results 13 mm. The produced AgNPs displayed highly strong antibacterial action against the target multidrug-resistant microorganisms.

Table 2 Antibacterial efficacy of manufactured AgNPs against clinical pathogenic microorganisms

S. no	Microorganisms	Positive (chloramphenicol)	Aqueous extract	Concentrations of AgNPs ($\mu\text{g/mL}$)		
				25	50	75
				(ZONE OF INHIBITION in mm)		
1	<i>S. pyogenes</i>	12 ± 0.9	10 ± 0.9	10 ± 0.8	$15 \pm 0.8^{**}$	$16 \pm 0.0^*$
2	<i>E. coli</i>	$11 \pm 0.5^{**}$	$11 \pm 0.4^*$	$11 \pm 0.8^{**}$	14 ± 0.9	15 ± 0.9
3	<i>V. cholerae</i>	$12 \pm 0.6^*$	$10 \pm 0.8^*$	$12 \pm 0.6^*$	15 ± 0.8	18 ± 0.8
4	<i>S. aureus</i>	12 ± 0.8	13 ± 0.6	13 ± 0.4	$15 \pm 0.4^*$	$17 \pm 0.8^*$
5	<i>K. pneumoniae</i>	11 ± 0.4	12 ± 0.8	12 ± 0.8	$4 \pm 0.8^{**}$	$16 \pm 0.4^*$

ANOVA followed by Tukey's HSD post hoc test. The outcomes are statistically significant at the level ($*p \leq 0.01$, $**p \leq 0.001$), and other values are not statistically significant)

When compared to other multidrug-resistant bacteria, the MIC range of test AgNPs was 4.50 mg/mL at the lowest concentration of *V. trifolia* leaf extract against *S. aureus* (Table 3). The MIC dilutions were grown on sterile Muller-Hinton agar plates to calculate MBC. In treating AgNPs, the treatment concentration is where there is no growth on agar. When coated with AgNPs, MBC values in *S. aureus* and *E. coli* were 4.5 mg/mL and 8 mg/mL, respectively, followed by other pathogenic strains.

3.5 Protein leakage assay

At the time of the investigation, silver nanoparticle-treated bacterial cells leaked nearly as much protein as control cells. However, the untreated cells showed the same levels of protein leakage. The bacterial cells treated with silver nanoparticles exhibited more than three times the permeability of the control cells 6 h after incubation. Remarkably, at 6 h following treatment with AgNPs, *S. pyogenes*, *S. aureus*, and *K. pneumoniae* cells displayed the largest quantity of protein leakage, followed by (95 µg/mL), (92 µg/mL), (90 µg/mL), and then other species (Fig. 6a).

3.6 Nucleic acid leakage assay

Following exposure to AgNPs at different time points, the optical density at 260 nm of the cell-free filtrate was utilized to measure the leakage of intracellular components. Nanoparticle-treated cells and control cells initially leaked approximately the same amounts of nucleic acid. Increased nucleic acid release was triggered by the treatment of bacterial cells with AgNPs, and it was most prominent in *S. pyogenes*, *E. coli*, *S. aureus*, *V. cholerae*, and *K. pneumoniae*. However, the bacterial cells in the control group functioned worse than those exposed to silver nanoparticles, respectively (Fig. 6b).

3.7 In vitro killing assay

The killing kinetic test was performed to assess post-treatment bacterial viability and to determine the shortest time needed to achieve an inhibitory or bactericidal impact because there was no noticeable difference in the

bactericidal effects of AgNPs on the various bacteria. The time-kill curve of AgNPs against *S. pyogenes*, *V. cholerae*, *E. coli*, *S. aureus*, and *K. pneumoniae* strains is presented in (Fig. 6c). When exposed to AgNPs for 8 h at the suitable MBC concentrations for both strains (using the McFarland Standard), bactericidal activity steadily increased, and the whole bacterial population was destroyed during this time. AgNPs showed time-dependent and rapid bactericidal activity against tested pathogens, leading to premature stationary phase.

3.8 AgNPs antioxidant activity

The antioxidant activity of fabricated AgNPs, aqueous extract, and reference (ascorbic acid) was assessed at various concentrations (50–250 µg/mL) using the DPPH and reducing power test. Nanoparticles scavenged both radicals' dose-dependently (Fig. 7a). The biologically synthesized AgNPs observed ability to scavenge DPPH via aqueous extract was $18.24 \pm 0.45\%$ at the highest concentration (250 µg/mL), whereas the AgNPs were found to be $85.1 \pm 20.5\%$. Ascorbic acid inhibited $98 \pm 0.08\%$ at the same dose. AgNPs inhibit $90.23 \pm 0.5\%$ of reducing power at 250 µg/mL. Likewise, aqueous extract showed the inhibition percentage was $15.04 \pm 1.0\%$. Furthermore, the reference inhibition percentage at the same concentration was $99.7 \pm 50.5\%$ (Fig. 7b–c). According to both assay percentages (%), AgNPs made using *V. trifolia* and having tiny particles exhibited the highest level of antioxidant activity when compared to aqueous extract.

3.9 Photocatalytic activity of synthesized AgNPs against organic dye methylene blue

In this study, manufactured AgNPs were used as a nano catalyst to remove organic hazardous dyes more rapidly and easily while exposed to visible light. The photocatalytic degradation of methylene blue was examined utilizing green produced AgNPs and solar irradiation methods. The color change from a dark to a light color during a range of incubation times (0–3 h) with AgNPs exposed to solar irradiation acts as the main indication of dye degradation. The characteristic absorption peaks for methylene blue at 550 nm, respectively (Fig.S1). The percentage of dye degradation was increased with increasing the exposure time and data were represented (Fig.S2). The exposure of synthesized AgNPs at (250 µg/mL) concentration demonstrated 95% photocatalytic activity over a 2.30-h period. The results strongly suggest that the dye concentration in the solution decreased progressively as the exposure periods increased, confirming that the nanoparticles possess photocatalytic degradation activity. The reaction kinetics of *V. trifolia*

Table 3 MIC and MBC values of AgNPs against tested pathogens

Sl. no	Microbial strains	MIC (µg/mL)	MBC (µg/mL)
1	<i>S. aureus</i>	3.12	4.5
2	<i>E. coli</i>	3.12	10.2
3	<i>S. pyogenes</i>	4.25	13.1
4	<i>V. cholerae</i>	6.20	8.2
5	<i>K. pneumoniae</i>	5.23	10.1

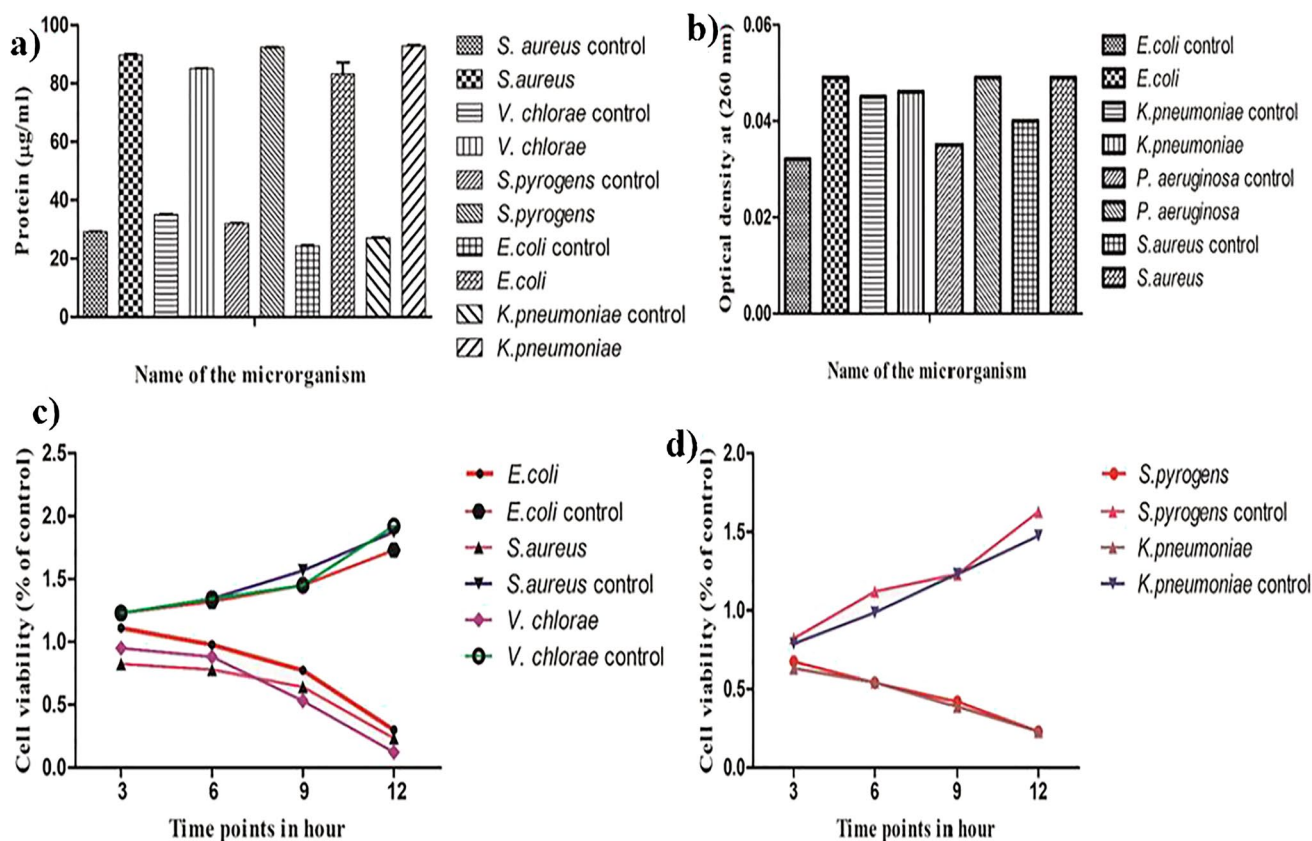


Fig. 6 Cellular contents measurements: **a)** protein leakage assay, **b)** nucleic acid leakage, **c)** in vitro killing assay

AgNPs displays the dye model reaction as pseudo-first-order kinetics, with the rate constant of MB dye degradation by AgNPs (100, 150, 200 µg/mL with H₂O₂) and H₂O₂ alone as 0.005180, 0.005491, 0.01127, and 0.003712 min⁻¹ (Fig.S3 & S4). The photo-irradiation catalyzed dye MB degradation experimented for six cycles, demonstrating the stability of AgNPs even after six cycles with the degradation efficiency of 95%.

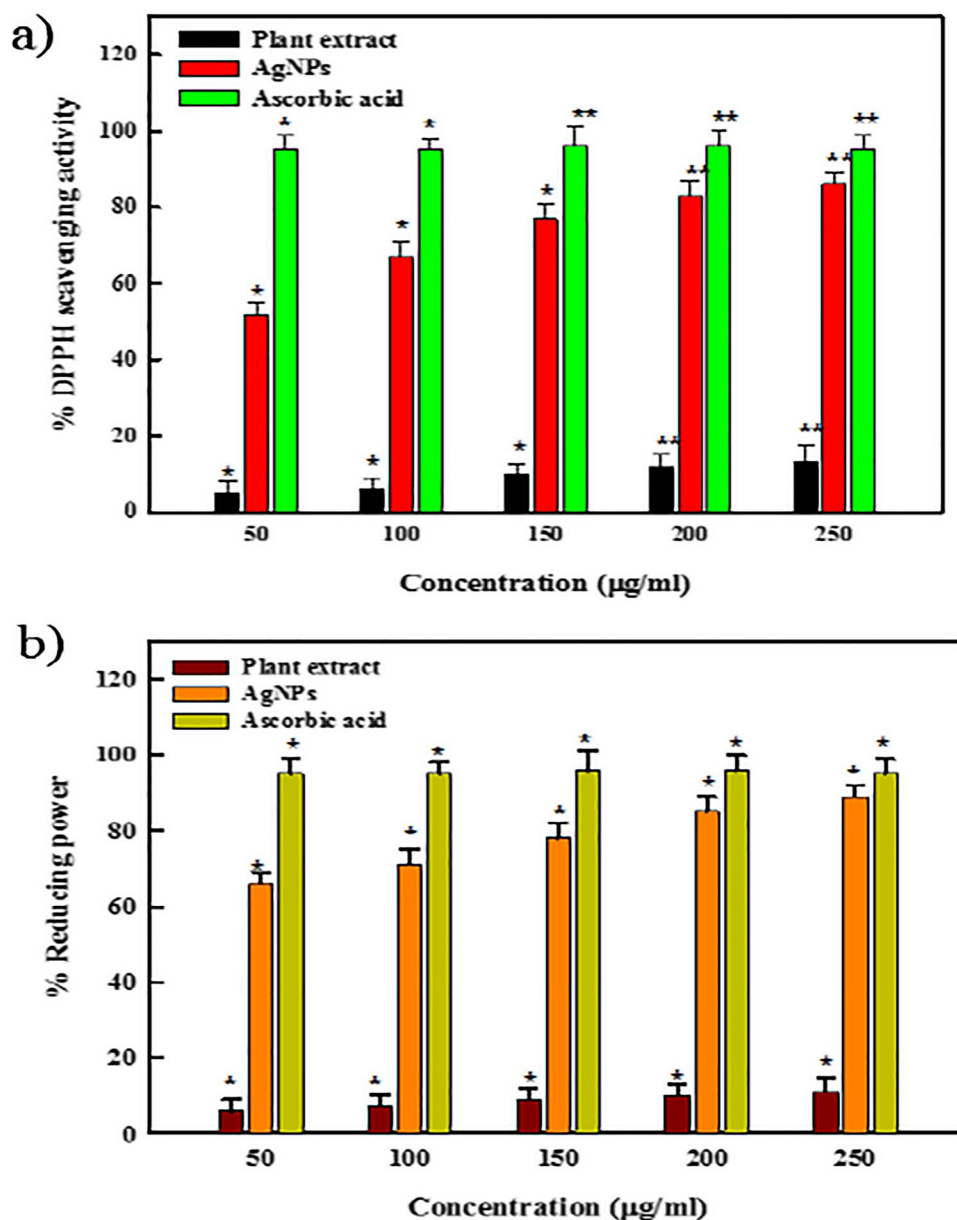
The current results showed AgNPs toxicity to living organisms and growth inhibition in aquatic and terrestrial environments. Different concentrations of manufactured AgNPs were exposed to *C. vulgaris* algae. The increasing concentration of AgNPs caused a decrease in algae growth. Furthermore, when exposed to synthesized AgNPs, the data confirmed a concentration-dependent increase in growth inhibition rate. Chlorophyll *a* and *b* concentrations are depicted in (Fig. 8a-b). The amount of chlorophyll *a* and *b* in the control algae was the same after exposure to AgNPs, but this level drastically decreased ($p \leq 0.01$). At the maximum concentration tested (250 µg/mL), chlorophyll *a* and *b* were noticed at 55% and 46%, respectively, compared to the control (Fig. 9a-b). The shape of the algal cells changed substantially after exposure to AgNPs. After being exposed to AgNPs MDA profile, *C. vulgaris* lipid peroxide levels

elevated to 1.5- to 4.5-fold that the control, respectively. The outcome suggested that *C. vulgaris* could sustain more severe oxidative damage from AgNPs produced by *V. trifolia*. When exposed to *V. trifolia*-manufactured AgNPs, *C. vulgaris* had notably higher glutathione (GSH) than the control group (Fig. 8c), which is in accordance with the activities of antioxidant enzymes. Additionally, one-way ANOVA findings showed that MDA and GSH concentrations in the exposure treatment were notably greater than those in the control, demonstrating that AgNPs exposure progressively raised MDA and GSH content in *C. vulgaris* (Fig. 8b).

4 Discussion

Silver nitrate (AgNO₃) was used to produce AgNPs from *V. trifolia* leaf extract. After a certain amount of time, the reaction medium's color changed immediately when AgNPs were synthesized and fabricated. Ag⁺ was reduced, which resulted in an increase in color intensity over time. The silver nitrate solution changed from being colorless to a darkish brown after the biomass was added. Dried biomass plays a vital role in the synthesis of AgNPs and the color change in solutions is due to surface Plasmon vibrations with AgNPs

Fig. 7 Antioxidant assays of synthesized AgNPs **a)** DPPH scavenging assay, **b)** ferric reducing power assay. A single asterisk (*) indicates a significant difference between the positive control (ascorbic acid) and test samples at $P < 0.05$, double asterisk (**) at $P < 0.01$. Values are mean \pm SD



[66]. UV–visible spectrophotometry was used to confirm the NPs production. The color was produced via the stimulation of surface plasmon vibrations, which are typical of AgNPs and have maximum reported values in the visible range of 400–450 nm [67].

The FTIR spectra of *V. trifolia* synthesized AgNPs showed transmittance peaks at aliphatic groups. These peaks demonstrate that an amino acid residue cap on the silver nanoparticles produces a methyl group, which prevents agglomeration and regulates the medium [68]. Plant phytochemicals and secondary metabolites are considered as reducing agents in the green synthesis. The extract carbonyl functional clusters form flavonoids to interact with metallic ions, providing reactive hydrogen that causes the flavonoid enol to shift to keto form and probably produce Ag [69].

The functional groups of the fabricated AgNPs were identified via FTIR analysis. Alcohol, amines, amides, alkanes, methyl, aliphatic, and halide functional groups, which are the main classes in the majority of functional groups, were found in AgNPs. Similar findings have been made, which indicate potential biomolecules in charge of the AgNPs' stabilizing, capping, and reducing agents [70]. Additionally, Ajitha et al. [71] reported that the biogenic synthesis of AgNPs from *Tephrosia purpurea* revealed various functional groups via alkanes and aliphatic amine groups. Recently, Bhuyar et al. [72] investigated the *Padina* sp.-synthesized AgNPs and exhibited different function groups such as nitro compounds, alkynes, aliphatic amines, and primary and secondary amines, which played a crucial role in the capping and stabilizing of NPs.

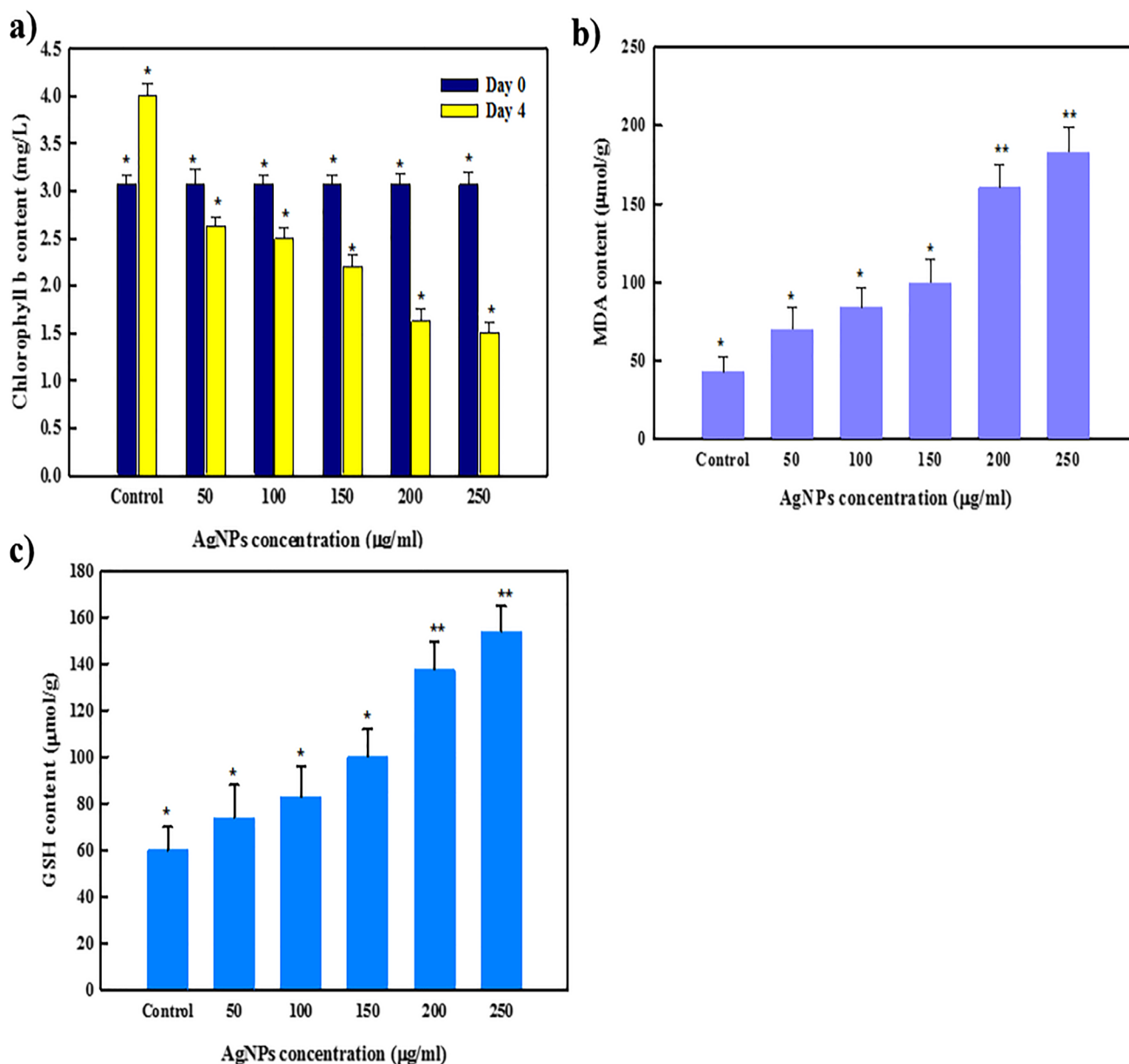


Fig. 8 Algae growth percentage of *C. vulgaris* exposed to different concentration of AgNPs. **a)** and **b)** Content of chlorophyll *a*, **b)** MDA content analysis, **c)** GST assay. A single asterisk (*) indicates a sig-

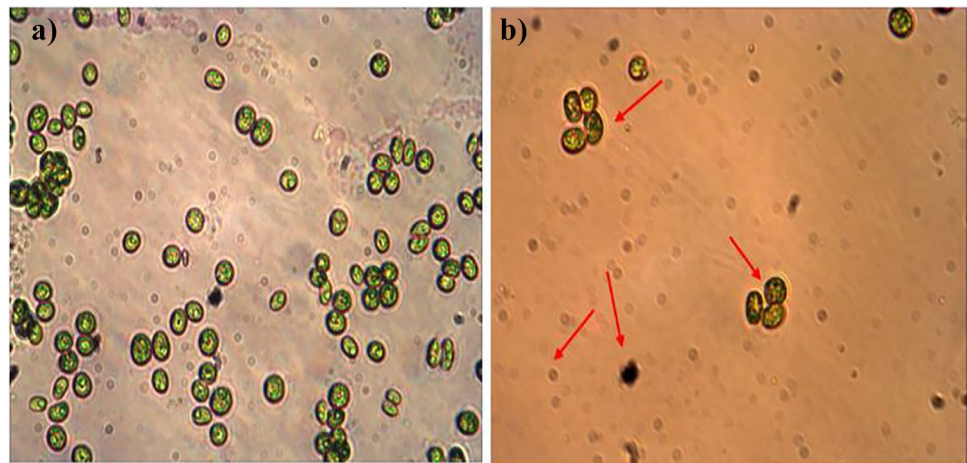
nificant difference between the positive control (ascorbic acid) and test samples at $P < 0.01$., double asterisk (**) at $P < 0.001$. Values are mean \pm SD

The 111, 200, 220, 311, and 222 crystallographic planes have XRD peaks at 38.17° , 44.31° , 64.44° , and 77.34° . Similar peak values showed that bio-organic crystallization occurred on silver nanoparticles [73]. The composition of silver metals is observed to be the major component present in silver nanoparticles at about 59%. The presence of metallic silver was indicated by the strong peak at 3 keV. This also demonstrates that *F. indica* extracts could be employed to successfully produce AgNPs [74]. The figures showed that there were well-defined spherical SNPs without any aggregation. The average particle size in the TEM image of the

selected site was 50 nm, which is within the nano-range. Similarly, *A. nilagirica* leaf extract-mediated silver nanoparticles reported by Vijayakumar et al. [75]. According to the TEM image, the fabricated AgNPs had a size range of 50–200 nm, and the majority of them had a spherical structure. The average AgNPs size was 24 nm, with particle sizes ranging from 50 to 190 nm [76]. Interestingly, Dogiparthi et al. [77] investigated that phytochemical mediated produced AgNPs had an average nanoparticle size of 20–50 nm.

The current study found that the maximum antibacterial activity was an 18-mm diameter zone of inhibition exhibited

Fig. 9 *C. vulgaris* microscopic view of **a)** control algae; **b)** treatment of AgNPs at 250 $\mu\text{g}/\text{mL}$. Red arrow indicates ‘cell injury’



against *V. cholerae*, followed by a 17-mm diameter zone of inhibition observed against *S. aureus* when compared to the reference chloramphenicol. Metallic silver would also be a strong antibacterial agent with high potential activity. The high reactivity and maximum binding affinity with proteins are achieved by modifying the structure of the bacterial cell wall and nuclear membrane, resulting in cell disintegration and damage. AgNPs with a diameter ranging from 20 to 100 nm exhibited strong bactericidal action against Gram positive and negative bacteria [78]. When bacteria were exposed to AgNPs for 6 h at their respective MBC concentrations for both strains, bactericidal activity steadily increased, and the whole bacterial population was destroyed during this time. According to the results of our investigation, silver nanoparticles effectively inhibited bacterial growth in a dose-and time-dependent manner.

The growth curves of bacteria exposed to AgNPs showed that it might prevent bacterial growth and reproduction [79]. The broth culture of selected bacteria was utilized to measure the MIC values of biogenic AgNPs. AgNPs displayed higher bacterial growth inhibitory action against *S. aureus* and *E. coli* (MIC 6.25 and 3.12 $\mu\text{g}/\text{mL}$) than *V. cholerae* and *K. pneumoniae* (MIC 5.23 and 6.20 $\mu\text{g}/\text{mL}$). The absorbance (λ_{max} 600) decreased with nanoparticle concentration for all bacterial strains [1]. In the case of treatment with AgNPs, the drug concentration was found at a stage where no observable growth was visible on the agar plate. When loaded with AgNPs, the MBC values of *S. aureus* (4.2 $\mu\text{g}/\text{mL}$) and *E. coli* (8.2 $\mu\text{g}/\text{mL}$) were the highest, followed by other strains [51].

AgNPs-treated bacterial cells released nearly as much protein as control cells at the start of the experiment. After 3 h, treated cells leaked 35–43 mg/mL protein. Interestingly, Balakumaran et al. [52] reported that the silver nanoparticles tested against *E. faecalis*, *P. aeruginosa*, and *B. subtilis* cells showed the highest amount of protein leakage (99 $\mu\text{g}/\text{mL}$) followed by (90 $\mu\text{g}/\text{mL}$) and (89 $\mu\text{g}/\text{mL}$) at 6 h after treatment. The increase in OD at (260 nm) signifies a loss

in membrane integrity and is caused by the leakage of intracellular nucleic acids. According to the earlier report [71], AgNPs may cause cytoplasmic membrane pores by causing the leakage of intracellular components. Overall, these findings strongly imply that silver nanoparticles directly interact with bacteria since the membrane shape was significantly altered [80].

A DPPH scavenging and ferric reducing assay was used to evaluate the antioxidant activity of the aqueous extract and fabricated AgNPs. The data implies that naturally produced AgNPs had superior antioxidant activity than extracts. Furthermore, a dose-dependent increase in inhibition percentage (%) was found for the lowest concentration (50 $\mu\text{g}/\text{mL}$) of aqueous extract (5.34%) and for 250 $\mu\text{g}/\text{mL}$ (18.62%). However, for AgNPs, the percent inhibition values at 50 and 250 $\mu\text{g}/\text{mL}$ concentrations were 46.32% and 88.28%, respectively. Earlier, Parveen et al. [81] investigated the *Fraxinus excelsior* leaf extract-mediated synthesized AgNPs showed prominent antioxidant properties at the lowest concentration. Synthesized AgNPs showed promising DPPH free radical scavenging activity compared to ascorbic acid. Similarly, Netala et al. [82] demonstrated 55% inhibition in a DPPH radical scavenging assay at 50 $\mu\text{g}/\text{mL}$ employing AgNPs manufactured by endophytic fungi. Biological systems may defend themselves from reactive oxygen species (ROS) such as hydrogen peroxide, singlet oxygen, or hydroxyl radicals via antioxidants [83]. AgNPs produced from *Vigna mungo* seed extract showed in vitro antioxidant efficacy against DPPH radicals with the highest inhibition of (75%), respectively [84]. Additionally, Saratale et al. [85] observed that *Punica granatum* leaf synthesized AgNPs demonstrated DPPH scavenging capacity with an IC_{50} value of 67.1 $\mu\text{g}/\text{mL}$.

Synthetic dyes are used in many items, including paper, textiles, glues, cosmetics, food, ink, and pharmaceuticals [86]. A heterocyclic azo dye called methylene blue (MB) is frequently discharged into the environment by the textile

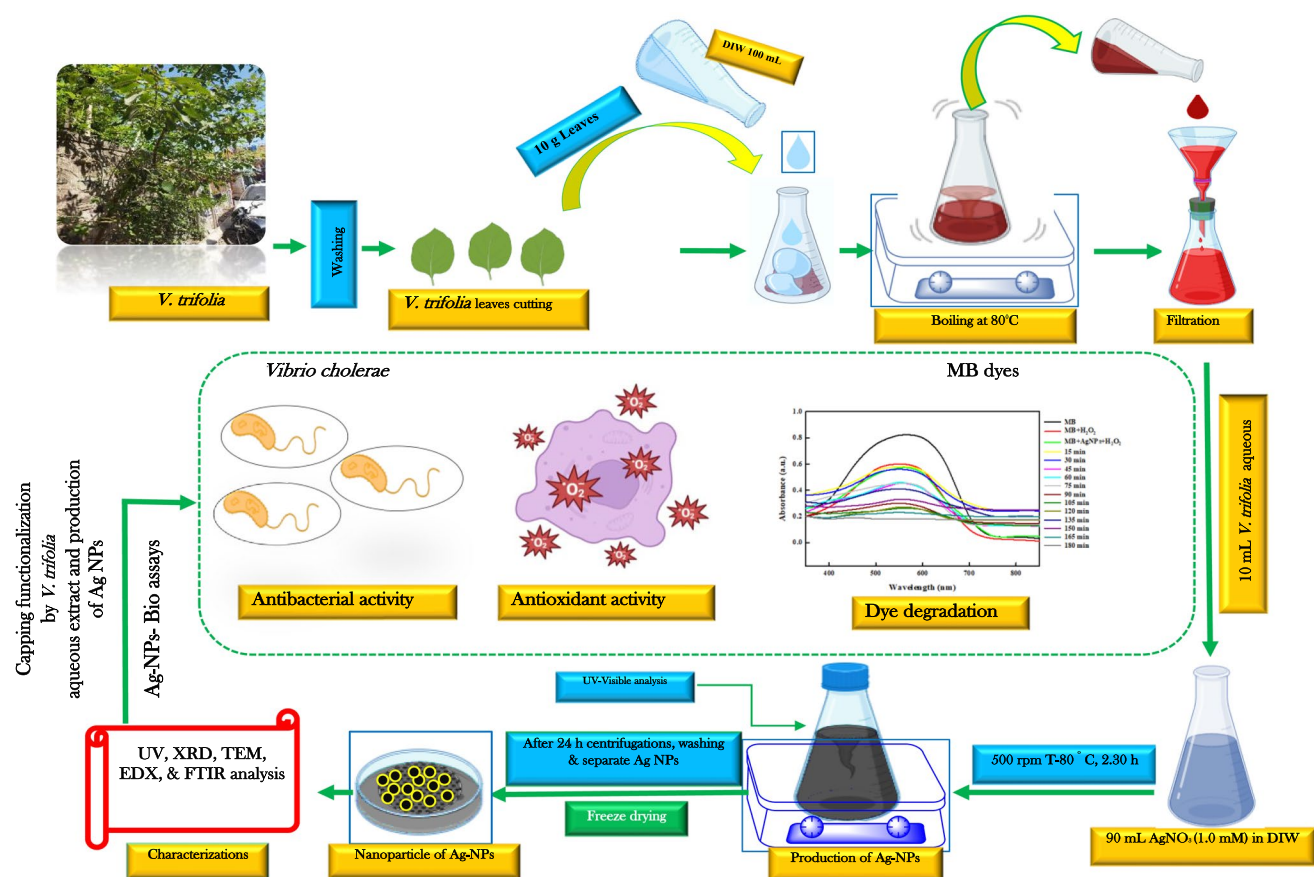


Fig. 10 Illustrations for the productions of biogenic AgNPs, their characterization, and capping evaluations using various protocol in combination with *V. trifolia* aqueous extract

industry. It reduces the amount of oxygen on the surface of bodies of water, which has an impact on aquatic vegetation, wildlife, and human toxicity. To the best of our knowledge, the current study, the first report on the MB photocatalytic activity of biosynthesized AgNPs. After the addition of the nanoparticle, the MB solution changed color clearly. At first, the color of the MB solution was deep blue, but after the addition of nanoparticles, it turned dark green. The degree of MB degradation was determined to be centered at 550 nm. The sun-exposed control MB solution did not alter color. Additionally, the MB absorption band was shown to decrease significantly in the presence of AgNPs. The maximum percentage of nanoparticle-fabricated MB dye degradation was observed to be 95% at 150 min. Similarly, Kadam et al. [87] observed the synthesized AgNPs from cauliflower waste exhibited methylene blue degradation at 97% at 150 min. The result that AgNPs mediated a considerable reduction in phenol demonstrates that AgNPs increase photocatalytic degradation. The methylene blue molecule interacts in a liquid state to produce degradation products, according to the Eley–Rideal mechanism, which

is an indirect method of reaction. The production of hole-electron pairs in the valence band and conduction band as a result of irradiating the catalyst is however taken into consideration in this process. The production of the OH radical and H⁺ is caused by the water molecule binding the gap created in the catalyst's valence band. The molecular oxygen traps the photoexcited electron in the conduction band, forming superoxide anion, which can set off a sequence of reactions to generate HO radicals. Finally, the OH radicals attack the methylene blue molecule and yield intermediates and end products [88]. Additionally, Sivaramkrishnan et al. [89] studied the synthesized AgNPs from *Leucas aspera* revealed the degradation of optilan red and lanasyn blue absorption peaks were found to be 246 and 626 nm. Similarly, Ganapathy Selvam and Sivakumar [90] demonstrated that solar light decolorized methyl orange more quickly than alternative irradiation methods, as seen by a drop in peak intensity after 10 h. Figure 10 shows the schematic for the entire synthesis of biogenic AgNPs, their characterization, and capping confirmation using various methods in combination with *V. trifolia* aqueous extract.

5 Conclusion

The present study demonstrates an effective green approach for producing AgNPs employing *V. trifolia* leaf extract as the bio-reductant. Physical measurements suggested that the synthesized nanoparticles were very small in size and highly pure in nature, where plant products such as polyphenols, flavonoids, and proteins served as capping and stabilizing agents. Multidrug-resistant pathogens were used to evaluate the antibacterial activity of the nanoparticles. It was demonstrated that AgNPs showed antibacterial activity and higher effectiveness was found against *S. aureus* and *E. coli*. The bacterial killing mechanism damages the cell membrane, followed by a protein leakage assay. This nanomaterial is another option for the treatment of multidrug-resistant bacterial infections. The synthesized AgNPs demonstrated a promising ability to diffuse the damaging free radicals and might be used as a food additive as well as in the nutraceutical and bio-pharmaceutical industries. Moreover, the biomolecule capped AgNPs revealed that the nanoparticle strongly degrades the industrial organic coloring stain such as methylene blue. In summary, in this study, we demonstrate the ability of AgNPs to reduce the growth rate, alter the photosynthetic pigments, and their antioxidant enzyme in *C. vulgaris*. Overall, the obtained data demonstrated that synthesized AgNPs from *V. trifolia* could be used as potent nanodrugs against human clinical pathogens, free radical scavenging, and to efficiently degrade the organic dye from the textile industry and remove environmental pollution in the future.

Supplementary Information The online version contains supplementary material available at <https://doi.org/10.1007/s13399-022-03705-5>.

Acknowledgements The authors gratefully acknowledge the Department of Biotechnology, Periyar University, Salem, India for providing all the infrastructural facilities and financial assistance. The authors are also grateful to SAIF, IIT-Madras, Chennai for their analytical facilities. The taxonomic identification of the plant was confirmed by Dr. Arulbalachandran, Assistant Professor, Department of Botany, Periyar University, Salem, Tamil Nadu.

Author contribution CR: designed the experiment, carried out the experiment, and approved the final version of the manuscript. TC and AP: performed photocatalytic activity. NM: isolation and identification of MDR bacteria, formal analysis. BG: performed statistical analysis, methodology. TK and CK: studied the antibacterial activity, methodology. CR, JK, and SS: conducted the algae experiment, CR, and PW: coordination of overall studies. All authors have approved the final version of the manuscript.

Funding The Council for Scientific and Industrial Research (CSIR), Government of India, New Delhi, is thanked for the released grant (Ref. Lr. 09/810 (0024)/2016-EMR-I) under the CSIR-SRF (Direct) Research Fellowship. This work was partially supported by Leiden University.

Data availability All data generated or analyzed during this study are included in this article.

Declarations

Competing interest The authors affirm that they have no known financial or interpersonal conflicts that would have appeared to have an impact on the research presented in this study.

References

1. Yang M, Zhang M, Wang Y et al (2022) Silver nanoparticle-loaded gelatin-based nanocomposite films toward enhanced mechanical properties and antibacterial activity. *ACS Appl Mater* 5:2193–2201
2. Shanmuganathan R, MubarakAli D, Prabakar D et al (2018) An enhancement of antimicrobial efficacy of biogenic and ceftriaxone-conjugated silver nanoparticles: green approach. *Environ Sci Pollut Res Int* 25:10362–10370
3. Michailidu J, Mařátková O, Kolouchová I, Masák J, Čejková A (2022) Silver nanoparticle production mediated by *Vitis vinifera* Cane Extract: characterization and antibacterial activity evaluation. *Plants* 11(3):443. <https://doi.org/10.3390/plants11030443>
4. Saravanan M, Barik SK, MubarakAli D et al (2018) Synthesis of silver nanoparticles from *Bacillus brevis* (NCIM 2533) and their antibacterial activity against pathogenic bacteria. *Microb Pathog* 116:221–226
5. Boutinguiza M, Comesaña R, Lusquinos F et al (2015) Production of silver nanoparticles by laser ablation in open air. *Appl Surf Sci* 336:108–111
6. Chinnasamy R, Chinnaperumal K, Venkatesan M, Jogikalmat K, Cherian T, Willie P, Malafaia G (2023) Eco-friendly synthesis of Ag-NPs using *Endostemon viscosus* (Lamiaceae): antibacterial, antioxidant, larvicidal, photocatalytic dye degradation activity and toxicity in zebrafish embryos. *Environ Res* 218(1):1–16
7. Srivastava V, Pandey S, Mishra A, Choubey AK (2019) Green synthesis of biogenic silver particles, process parameter optimization and application as photocatalyst in dye degradation. *SN Applied Sciences* 1:1722
8. Rajput S, Kumar D, Agrawal V (2020) Green synthesis of silver nanoparticles using Indian *Belladonna* extract and their potential antioxidant, anti-inflammatory, anticancer and larvicidal activities. *Plant Cell Rep* 39:921–939
9. Elumalai D, Hemavathi M, Rekha GS et al (2021) Photochemical syntheses of silver nanoparticles using *Oscillatoria sancta* micro algae against mosquito vectors *Aedes aegypti* and *Anopheles stephensi*. *Sens Bio-Sens Res* 34:100457
10. Patil MP, Kim G-D (2017) Eco-friendly approach for nanoparticles synthesis and mechanism behind antibacterial activity of silver and anticancer activity of gold nanoparticles. *Appl Microbiol Biotechnol* 101:79–92
11. Makarov VV, Makarova SS, Love AJ et al (2014) Biosynthesis of stable iron oxide nanoparticles in aqueous extracts of *Hordeum vulgare* and *Rumex acetosa* plants. *Langmuir* 30:5982–5988
12. Devatha CP, Thalla AK, Katte SY (2016) Green synthesis of iron nanoparticles using different leaf extracts for treatment of domestic waste water. *J Clean Prod* 139:1425–1435
13. Aisida SO, Madubuonu N, Alnasir MH et al (2020) Biogenic synthesis of iron oxide nanorods using *Moringa oleifera* leaf extract for antibacterial applications. *Appl Nanosci* 10:305–315
14. Madubuonu N, Aisida SO, Ahmad I et al (2020) Bio-inspired iron oxide nanoparticles using *Psidium guajava* aqueous extract for antibacterial activity. *Appl Phys A: Mater Sci Process* 126:72

15. de Kok RPJ (2007) The genus *Vitex* L. (Lamiaceae) in New Guinea and the South Pacific Islands. Kew Bull 62:587–603
16. Holdsworth (1977) Medicinal plants of Papua New Guinea, South Pacific Commission Technical Paper No. 175. New Caledonia Noumea, pp 92–94
17. Kannathasan K, Senthilkumar A, Chandrasekaran M, Venkatesalu V (2007) Differential larvicidal efficacy of four species of *Vitex* against *Culex quinquefasciatus* larvae. Parasitol Res 101:1721–1723
18. Hossain MM, Paul N, Sohrab MH et al (2001) Antibacterial activity of *Vitex trifolia*. Fitoterapia 72:695–697
19. Woradulayapinij W, Soonthornchareonnon N, Wiwat C (2005) In vitro HIV type 1 reverse transcriptase inhibitory activities of Thai medicinal plants and *Canna indica* L. rhizomes. J Ethnopharmacol 101:84–89
20. Hernández MM, Heraso C, Villarreal ML et al (1999) Biological activities of crude plant extracts from *Vitex trifolia* L. (Verbenaceae). J Ethnopharmacol 67:37–44
21. Ikram M, Khattak SG, Gilani SN (1987) Antipyretic studies on some indigenous Pakistani medicinal plants: II. J Ethnopharmacol 19:185–192
22. Wang Q, Wangjin X, Zhang Y et al (2020) The toxicity of virgin and UV-aged PVC microplastics on the growth of freshwater algae *Chlamydomonas reinhardtii*. Sci Total Environ 749:141603
23. Shang J, Zou W, Wang P et al (2021) Preparation and characterization of hollow zinc oxide nanofibers and investigation of its photocatalytic properties. J Nanoelectron Optoelectron 16:64–71
24. Panimalar S, Uthrakumar R, Selvi ET et al (2020) Studies of MnO₂/g-C₃N₄ heterostructure efficient of visible light photocatalyst for pollutants degradation by sol-gel technique. Surf Interfaces 20:100512
25. Sharma S, Ibadon AO, Francesconi MG, Mehta SK, Elumalai S, Kansal S K, Baskoutas S (2020) Bi₂WO₆/C-Dots/TiO₂: a novel Z-scheme photocatalyst for the degradation of fluoroquinolone levofloxacin from aqueous medium. Nanomaterials 10(5):910. <https://doi.org/10.3390/nano10050910>
26. Kumar SA, Jarvin M, Imbanathan SSR et al (2022) Facile green synthesis of magnesium oxide nanoparticles using tea (*Camellia sinensis*) extract for efficient photocatalytic degradation of methylene blue dye. Environ Technol Innov 28:102746
27. Ma W, Li L (2020) Visible light activity in phenol degradation of C60@P25 Photocatalyst with Core-Shell Structure. J Nanoelectron Optoelectron 15:189–196
28. Jing B, Ao Z, Zhao W et al (2020) Evaluation procedure of photocatalysts for VOCs degradation from the view of density functional theory calculations: g-C₃N₄ dots/graphene as an example. J Mater Chem A Mater Energy Sustain 8:20363–20372
29. Fang Y, Huang W, Yang S et al (2020) Facile synthesis of anatase/rutile TiO₂/g-C₃N₄ multi-heterostructure for efficient photocatalytic overall water splitting. Int J Hydrogen Energy 45:17378–17387
30. Nga NTA, Raghavendra VB, Sindhu R et al (2022) Green fabrication of silver nanoparticles using *Chloroxylon swietenia* leaves and their application towards dye degradation and food borne pathogens. Food Chem Toxicol 165:113192
31. Song WC, Kim B, Park SY et al (2022) Biosynthesis of silver and gold nanoparticles using *Sargassum horneri* extract as catalyst for industrial dye degradation. Arab J Chem 15:104056
32. Dihom HR, Al-Shaibani MM, Radin Mohamed RMS et al (2022) Photocatalytic degradation of disperse azo dyes in textile wastewater using green zinc oxide nanoparticles synthesized in plant extract: a critical review. J Water Process Eng 47:102705
33. Marimuthu S, Antonisamy AJ, Malayandi S et al (2020) Silver nanoparticles in dye effluent treatment: a review on synthesis, treatment methods, mechanisms, photocatalytic degradation, toxic effects and mitigation of toxicity. J Photochem Photobiol B 205:111823
34. Singh J, Dhaliwal AS (2020) Plasmon-induced photocatalytic degradation of methylene blue dye using biosynthesized silver nanoparticles as photocatalyst. Environ Technol 41:1520–1534
35. Huq MA, Ashrafudoulla M, Rahman MM, Balusamy S R, Akter S (2022) Green synthesis and potential antibacterial applications of bioactive silver nanoparticles: a review. Polymers 14(4):742. <https://doi.org/10.3390/polym14040742>
36. Mustapha T, Misni N, Ithnin NR, Daskum AM, Unyah NZ (2022) A review on plants and microorganisms mediated synthesis of silver nanoparticles, role of plants metabolites and applications. International Journal of Environmental Research and Public Health 19(2):674. <https://doi.org/10.3390/ijerph19020674>
37. Ratte HT (1999) Bioaccumulation and toxicity of silver compounds: a review. Environ Toxicol Chem 18:89–108
38. Echavarri-Bravo V, Paterson L, Aspray TJ et al (2017) Natural marine bacteria as model organisms for the hazard-assessment of consumer products containing silver nanoparticles. Mar Environ Res 130:293–302
39. Sørensen SN, Baun A (2015) Controlling silver nanoparticle exposure in algal toxicity testing—a matter of timing. Nanotoxicology 9:201–209
40. Bruneau A, Turcotte P, Pilote M et al (2016) Fate of silver nanoparticles in wastewater and immunotoxic effects on rainbow trout. Aquat Toxicol 174:70–81
41. Macken A, Byrne HJ, Thomas KV (2012) Effects of salinity on the toxicity of ionic silver and Ag-PVP nanoparticles to *Tisbe battagliai* and *Ceramium tenuicorne*. Ecotoxicol Environ Saf 86:101–110
42. Safi C, Zebib B, Merah O et al (2014) Morphology, composition, production, processing and applications of *Chlorella vulgaris*: a review. Renew Sustain Energy Rev 35:265–278
43. Johari SA, Sarkheil M, Behzadi Tayemeh M, Veisi S (2018) Influence of salinity on the toxicity of silver nanoparticles (AgNPs) and silver nitrate (AgNO₃) in halophilic microalgae, *Dunaliella salina*. Chemosphere 209:156–162
44. Vinothkanna A, Mathivanan K, Ananth S et al (2022) Biosynthesis of copper oxide nanoparticles using *Rubia cordifolia* bark extract: characterization, antibacterial, antioxidant, larvicidal and photocatalytic activities. Environ Sci Pollut Res Int. <https://doi.org/10.1007/s11356-022-18996-4>
45. Rakesh B, Srinatha N, KJ RK et al (2022) Antibacterial activity and spectroscopic characteristics of silver nanoparticles synthesized via plant and in vitro leaf-derived callus extracts of *Mucuna pruriens* (L.) DC. S Afr J Bot 148:251–258
46. Jalab J, Abdelwahed W, Kitaz A, Al-Kayali R (2021) Green synthesis of silver nanoparticles using aqueous extract of *Acacia cyanophylla* and its antibacterial activity. Heliyon 7:e08033
47. Murugan N, Srinivasan R, Murugan A et al (2020) *Glycosmis pentaphylla* (Rutaceae): a natural candidate for the isolation of potential bioactive arborine and skimmianine compounds for controlling multidrug-resistant *Staphylococcus aureus*. Front Public Health 8:176
48. Murugan N, Natarajan D (2018) Bionanomedicine for antimicrobial therapy—a case study from *Glycosmis pentaphylla* plant mediated silver nanoparticles for control of multidrug resistant bacteria. Lett Appl NanoBioScience 8:523–540
49. Singh S, Bharti A, Meena VK (2015) Green synthesis of multi-shaped silver nanoparticles: optical, morphological and antibacterial properties. J Mater Sci: Mater Electron 26:3638–3648
50. Wiegand I, Hilpert K, Hancock REW (2008) Agar and broth dilution methods to determine the minimal inhibitory concentration (MIC) of antimicrobial substances. Nat Protoc 3:163–175
51. Das B, Dash SK, Mandal D et al (2017) Green synthesized silver nanoparticles destroy multidrug resistant bacteria via


- reactive oxygen species mediated membrane damage. Arab J Chem 10:862–876
52. Balakumaran MD, Ramachandran R, Balashanmugam P et al (2016) Mycosynthesis of silver and gold nanoparticles: optimization, characterization and antimicrobial activity against human pathogens. Microbiol Res 182:8–20
 53. Balakumaran RR, Jagadeeswari S, Kalaichelvan PT (2016) In vitro biological properties and characterization of nanosilver coated cotton fabrics – an application for antimicrobial textile finishing. Int Biodeterior Biodegradation 107:48–55
 54. Escárcega-González CE, Garza-Cervantes JA, Vázquez-Rodríguez A et al (2018) In vivo antimicrobial activity of silver nanoparticles produced via a green chemistry synthesis using *Acacia rigidula* as a reducing and capping agent. Int J Nanomedicine 13:2349–2363
 55. Gurunathan S (2019) Rapid biological synthesis of silver nanoparticles and their enhanced antibacterial effects against *Escherichia fergusonii* and *Streptococcus mutans*. Arab J Chem 12:168–180
 56. Manimaran K, Balasubramani G, Ragavendran C et al (2021) Biological applications of synthesized ZnO nanoparticles using *Pleurotus djamor* against mosquito larvicidal, histopathology, antibacterial, antioxidant and anticancer effect. J Cluster Sci 32:1635–1647
 57. Santhosh S, Manivannan N, Ragavendran C et al (2019) Growth optimization, free radical scavenging and antibacterial potential of *Chlorella* sp. SRD3 extracts against clinical isolates. J Appl Microbiol 127:481–494
 58. OECD (2011) 201: Freshwater alga and cyanobacteria, growth inhibition test. OECD guidelines for the testing of chemicals, Section 2(10.1787)
 59. Kusk KO, Christensen AM, Nyholm N (2018) Algal growth inhibition test results of 425 organic chemical substances. Chemosphere 204:405–412
 60. Jeffrey SW, Humphrey GF (1975) New spectrophotometric equations for determining chlorophylls a, b, c1 and c2 in higher plants, algae and natural phytoplankton. Biochem Physiol Pflanz 167:191–194
 61. Fazelian N, Movafeghi A, Yousefzadi M et al (2020) Impact of silver nanoparticles on the growth, fatty acid profile, and antioxidative response of *Nannochloropsis oculata*. Acta Physiol Plant 42:126
 62. Wang B, Zhang R, Xu J et al (2020) Effect of calcination temperature on light absorption and visible light photocatalytic activity of N doped TiO₂ nano-crystalline. Sci Technol Adv Mater 12:449–453
 63. Lu Q, Zhou W, Min M et al (2016) Mitigating ammonia nitrogen deficiency in dairy wastewaters for algae cultivation. Bioresour Technol 201:33–40
 64. Sun X, Zhong Y, Huang Z, Yang Y (2014) Selenium accumulation in unicellular green alga *Chlorella vulgaris* and its effects on antioxidant enzymes and content of photosynthetic pigments. PLoS ONE 9:e112270
 65. Melkamu WW, Bitew LT (2021) Green synthesis of silver nanoparticles using *Hagenia abyssinica* (Bruce) J.F. Gmel plant leaf extract and their antibacterial and anti-oxidant activities. Heliyon 7:e08459
 66. Składanowski M, Wypij M, Laskowski D et al (2017) Silver and gold nanoparticles synthesized from *Streptomyces* sp. isolated from acid forest soil with special reference to its antibacterial activity against pathogens. J Cluster Sci 28:59–79
 67. Jahan I, Erci F, Isildak I (2021) Rapid green synthesis of non-cytotoxic silver nanoparticles using aqueous extracts of “Golden Delicious” apple pulp and cumin seeds with antibacterial and antioxidant activity. SN Applied Sciences 3:94
 68. Dinesh D, Murugan K, Madhiyazhagan P et al (2015) Mosquitocidal and antibacterial activity of green-synthesized silver nanoparticles from *Aloe vera* extracts: towards an effective tool against the malaria vector *Anopheles stephensi*? Parasitol Res 114:1519–1529
 69. Alayande SO, Akinsiku AA, Akinsipo (Oyelaja) OB, et al (2021) Green synthesized silver nanoparticles and their therapeutic applications. In: Verma SK, Das AK (eds) Biosynthesized Nanomaterials. Elsevier, pp 585–611
 70. Lekha DC, Shanmugam R, Madhuri K et al (2021) Review on silver nanoparticle synthesis method, antibacterial activity, drug delivery vehicles, and toxicity pathways: recent advances and future aspects. J Nanomater 2021:1–11. <https://doi.org/10.1155/2021/4401829>
 71. Ajitha B, Reddy YAK, Reddy PS (2014) Biogenic nano-scale silver particles by *Tephrosia purpurea* leaf extract and their inborn antimicrobial activity. Spectrochim Acta A Mol Biomol Spectrosc 121:164–172
 72. Bhuyar P, Rahim MHA, Sundararaju S et al (2020) Synthesis of silver nanoparticles using marine macroalgae *Padina* sp. and its antibacterial activity towards pathogenic bacteria. Beni-Suef Univ J Basic Appl Sci 9:1–15
 73. Sathyavathi R, Krishna MB, Rao SV et al (2010) Biosynthesis of Silver nanoparticles using *Coriandrum sativum* leaf extract and their application in nonlinear optics. Adv Sci Lett 3:138–143
 74. Mehta BK, Chhajlani M, Shrivastava BD (2017) Green synthesis of silver nanoparticles and their characterization by XRD. J Phys Conf Ser 836:012050
 75. Vijayakumar M, Priya K, Nancy FT et al (2013) Biosynthesis, characterisation and anti-bacterial effect of plant-mediated silver nanoparticles using *Artemisia nilagirica*. Ind Crops Prod 41:235–240
 76. Thomas R, Janardhanan A, Varghese RT et al (2014) Antibacterial properties of silver nanoparticles synthesized by marine *Ochrobroctium* sp. Braz J Microbiol 45:1221–1227
 77. Dogiparthi LK, Sana SS, Shaik SZ et al (2021) Phytochemical mediated synthesis of silver nanoparticles and their antibacterial activity. SN Appl Sci 3:631
 78. Bresee J, Bond CM, Worthington RJ et al (2014) Nanoscale structure-activity relationships, mode of action, and biocompatibility of gold nanoparticle antibiotics. J Am Chem Soc 136:5295–5300
 79. Quintero-Quiroz C, Acevedo N, Zapata-Giraldo J et al (2019) Optimization of silver nanoparticle synthesis by chemical reduction and evaluation of its antimicrobial and toxic activity. Biomater Res 23:27
 80. Roy A, Bulut O, Some S et al (2019) Green synthesis of silver nanoparticles: biomolecule-nanoparticle organizations targeting antimicrobial activity. RSC Adv 9:2673–2702
 81. Parveen M, Ahmad F, Malla AM, Azaz S (2016) Microwave-assisted green synthesis of silver nanoparticles from *Fraxinus excelsior* leaf extract and its antioxidant assay. Appl Nanosci 6:267–276
 82. Netala VR, Kotakadi VS, Bobbu P et al (2016) Endophytic fungal isolate mediated biosynthesis of silver nanoparticles and their free radical scavenging activity and anti microbial studies. 3 Biotech 6:132
 83. Taha ZK, Hawar SN, Sulaiman GM (2019) Extracellular biosynthesis of silver nanoparticles from *Penicillium italicum* and its antioxidant, antimicrobial and cytotoxicity activities. Biotechnol Lett 41:899–914
 84. Soneya S, Reddy NV, Saritha KV, Kotakadi VS, Vijaya T (2019) Phytosynthesis of silver nanoparticles using *Rhynchosia heynei* wight & arn leaf extract: Characterization and in vitro assessment of antimicrobial, antioxidant and anticancer activities. In: International Conference on Nanomedicine. Springer, Cham, pp 120–140
 85. Saratale RG, Shin HS, Kumar G et al (2018) Exploiting antidiabetic activity of silver nanoparticles synthesized using *Punica granatum* leaves and anticancer potential against human liver cancer cells (HepG2). Artif Cells Nanomed Biotechnol 46:211–222

86. Indana M K, Gangapuram B R, Dadigala R, Bandi R, Guttena V (2016) A novel green synthesis and characterization of silver nanoparticles using gum tragacanth and evaluation of their potential catalytic reduction activities with methylene blue and Congo red dyes. *J Analytical Sci Techn* 7(1):1–9. <https://doi.org/10.1186/s40543-016-0098-1>
87. Kadam J, Dhawal P, Barve S, Kakodkar S (2020) Green synthesis of silver nanoparticles using cauliflower waste and their multifaceted applications in photocatalytic degradation of methylene blue dye and Hg²⁺ biosensing. *SN Appl Sci* 2:738
88. Saeed M, Muneer M, Akram N et al (2019) Synthesis and characterization of silver loaded alumina and evaluation of its photocatalytic activity on photo degradation of methylene blue dye. *Chem Eng Res Des* 148:218–226
89. Sivaramakrishnan M, Jagadeesan Sharavanan V, Karaiyagowder Govindarajan D et al (2019) Green synthesized silver nanoparticles using aqueous leaf extracts of *Leucas aspera* exhibits antimicrobial and catalytic dye degradation properties. *SN Appl Sci* 1:208
90. Ganapathy Selvam G, Sivakumar K (2015) Phycosynthesis of silver nanoparticles and photocatalytic degradation of methyl orange dye using silver (Ag) nanoparticles synthesized from *Hypnea musciformis* (Wulfen) J.V Lamouroux. *Appl Nanosci* 5:617–622

Publisher's note Springer Nature remains neutral with regard to jurisdictional claims in published maps and institutional affiliations.

Springer Nature or its licensor (e.g. a society or other partner) holds exclusive rights to this article under a publishing agreement with the author(s) or other rightsholder(s); author self-archiving of the accepted manuscript version of this article is solely governed by the terms of such publishing agreement and applicable law.

Authors and Affiliations

Ragavendran Chinnasamy^{1,2}  · Kamaraj Chinnaperumal³ · Priyadharsan Arumugam² · Murugan Natarajan¹ · Balasubramani Govindasamy⁴ · Krithikadatta Jogikalmat² · Tijo Cherian⁵ · Jothimani Kannupaiyan⁶ · Santhosh Sigamani⁷ · Peijnenburg Willie^{8,9}

¹ Natural Drug Research Laboratory, Department of Biotechnology, School of Biosciences, Periyar University, Periyar Palkalai Nagar, Salem 636 011, Tamil Nadu, India

² Department of Conservative Dentistry and Endodontics, Saveetha Dental College and Hospitals, Saveetha Institute of Medical and Technical Sciences (SIMATS), Chennai 600 077, India

³ Interdisciplinary Institute of Indian System of Medicine (IIISM), Directorate of Research and Virtual Education, SRM Institute of Science and Technology (SRMIST), Kattankulathur, Chennai 603203, Tamil Nadu, India

⁴ Department of Research and Innovation, Saveetha School of Engineering, Saveetha Institute of Medical and Technical Sciences (SIMATS), Chennai 602105, Tamil Nadu, India

⁵ Department of Ocean Studies and Marine Biology, Pondicherry University, Port Blair Campus, Brookshabad, Port Blair, Andamans 744112, India

⁶ Molecular and Stress Physiology Laboratory, Department of Botany, School of Life Sciences, Periyar University, Salem, Tamil Nadu, India

⁷ Department of Microbiology, School of Biosciences, Periyar University, Periyar Palkalai Nagar, Salem 636 011, Tamil Nadu, India

⁸ Institute of Environmental Sciences (CML), Leiden University, P.O. Box 9518, 2300 RA Leiden, The Netherlands

⁹ National Institute of Public Health and the Environment (RIVM), Center for Safety of Substances and Products, P.O. Box 1, Bilthoven, The Netherlands